

Titel: Cloud Top Height ATBD

Project: MAPP

Doc. No.: MAPP-ATBD-CTP

Issue: 1

Revision: 0

Date: 20.3.2000

	<u>Function</u>	<u>Name</u>	<u>Organisation</u>	<u>Signature</u>	<u>Date</u>
Author:		Jürgen Fischer, Rene Preusker, Lothar Schüller	FUB		

Internal Distribution

Name Organisation Quantity

External Distribution

Name Organisation Quantity

Change Record

Issue Revision Date Changes

Cloud Top Pressure

Jürgen Fischer, Rene Preusker, Lothar Schüller
Freie Universität Berlin
Institut für Weltraumwissenschaften

Table of Contents

1. INTRODUCTION	5
2. ALGORITHM OVERVIEW	6
3. ALGORITHM DESCRIPTION	8
3.1 THEORETICAL DESCRIPTION	8
3.1.1 <i>Physics of the Problem</i>	8
3.1.2 <i>Mathematical Description of the Algorithm</i>	11
3.1.2.1 Radiative Transfer Calculations	11
3.1.2.2 Neural Networks	12
3.1.2.3 Inversion	14
3.1.2.4 Generation of the <i>theoretical accuracy database</i>	15
3.1.2.5 Consistency check by estimation of the TOA radiance	16
3.2 PRACTICAL CONSIDERATIONS	16
3.2.1 <i>Numerical computation considerations</i>	16
3.2.2 <i>Calibration and Validation</i>	16
3.2.2.1 Quality Control, Diagnostics and Exception Handling	18
3.2.2.2 Output Products	18
4. ERROR BUDGET ESTIMATES AND SENSITIVITY TESTS	18
4.1 SENSITIVITY TO BAND SETTING AND TO SPECTRAL REGISTRATION	19
4.1.1 <i>Optimal band setting deduced from experimental data</i>	19
4.1.2 <i>Optimal band setting deduced from simulated data</i>	20
4.2 CLASSIFICATION OF THE CLOUD TOP PRESSURE ALGORITHM ERROR	22
4.2.1 <i>Absolute Calibration</i>	22
4.2.2 <i>Sensitivity to surface albedo and cloud optical thickness</i>	22
4.2.3 <i>Sensitivity to cloud optical thickness and cloud top pressure</i>	23
4.2.4 <i>Sensitivity of the cloud top pressure retrieval to viewing and solar zenith angle</i>	24
4.2.5 <i>MERIS swath simulation</i>	25
4.2.6 <i>Accuracy of the TOA radiance estimation</i>	26
5. ASSUMPTIONS AND LIMITATIONS	27
6. REFERENCES	27

1. INTRODUCTION

Clouds determine the amount of solar radiation scattered back into space as well as they block the terrestrial radiation from the earth's surface. An increase in globally averaged cloud top height of 1 km results in 1.2K increase in surface temperature (Ohring and Adler, 1978). Furthermore, a 1% change in cloud cover is estimated to have more than twice the effect of a CO_2 doubling (Ramanathan *et al.*, 1989). The most important cloud properties with respect to global climate change are the cloud amount, the cloud top height, the cloud optical thickness and the size of cloud droplets. However, only global observations of the cloud properties may serve global circulation model studies with sufficient input parameters to make them more realistic.

The most precise method for the detection of cloud top pressure from present infrared satellite measurements is the CO_2 *slicing technique* (Menzel, 1986). The accuracy of the most advanced techniques to derive cloud top heights is approximately within 500m. For climate studies and also for the improvement in the retrieval of vertical temperature profiles this accuracy has to be improved significantly.

For the retrieval of cloud top pressure we propose a method, based on reflected solar radiances of a few nanometers within the oxygen A-band absorption centred at $\lambda=761\text{nm}$. This method was first proposed by Yamamoto and Wark (1961). Besides theoretical investigations, airborne measurements have shown that the cloud top pressure and the cloud optical thickness can be inferred from multi channel measurements of the reflected solar radiation (Wu, 1985; King, 1987; Nakajima and King, 1988; Fischer *et al.*, 1991).

There have been only a few aircraft and satellite experiments for the retrieval of the cloud top pressure from measurements in the O_2 A-band in the last 20 years. Due to instrumental as well as theoretical problems the errors of the estimated cloud top pressures were in the same range as other operational techniques. (O'Brien and Mitchell, 1992). Cloud top pressure was successfully derived from measurements taken from an aircraft (Fischer *et al.*, 1991). The accuracy of the estimated cloud top height was within 40m above a stratocumulus deck with regard to simultaneously taken LIDAR measurements. Further investigations indicate that cloud top pressure can globally be achievable within $\pm 25\text{hPa}$ (Fischer and Kollewe, 1994; O'Brien and Mitchell, 1992). These results are based on theoretical investigations as well as aircraft measurements above various types of clouds. Additional aircraft measurements, such as those taken during the CIVEX campaign 1995 (Bakan *et al.*, 1998), are necessary to study a wide variety of physical effects and to validate detection procedures derived from theoretical calculations.

The most commonly used techniques for the remote sensing of atmospheric properties are based on Look Up Tables or simple regression methods. Artificial neural networks are capable to represent complex multidimensional relationships also. Since Rumelhart and McClelland (1986) introduced a learning scheme for artificial neural networks these techniques have been successfully adapted to remote sensing (Lee *et al.*, 1990; Churnside *et al.*, 1994). Such a technique is applied to interpret multispectral radiances within the O_2A absorption with respect to cloud top pressure.

2. ALGORITHM OVERVIEW

A schemata of measuring the cloud top pressures is illustrated in Figure 1. The sunlight reaching the cloud top, is backscattered and a part finally reaches the sensor on board a satellite. For a well mixed atmospheric gas like oxygen and a known vertical profile of the pressure and the temperature the penetrated air mass can be estimated by radiance measurements within an absorption band. For monochromatic light in a non-scattering atmosphere the relation between the amount of absorption and the penetrated air mass can be described by Lamberts law.

However, this simple approach is not sufficient because it does neither include scattering of radiation inside and outside the cloud nor describes the absorption of non-monochromatic light correct. The impact of micro physical cloud properties, varying cloud optical thickness, surface albedo as well as the observation geometry on the radiances can be investigated by radiative transfer simulations only. For the development and definition of a cloud top pressure algorithm the use of radiative transfer models is of advantage for a systematic analysis of the influence of cloud and surface properties as well as of the influence of measurement errors.

Since no simple relationship nor analytical formulation of the coherence between the radiances at top of atmosphere and cloud top pressure exists, radiative transfer simulations are used to establish an appropriate algorithm. There are different mathematical methods to solve the inverse problem. An approach, based on a complete radiative transfer code is not efficient enough with respect to computer time (Kollewe and Fischer, 1994). Faster semi-empirical radiative transfer codes have deficits with respect to accuracy. Neural networks are able to reduce the size of the required database and the operational computation times drastically. Matrices derived from a supervised learning procedure using simulation results, relate a vector of input information to a vector of cloud properties of interest. They are able to account for the non-linear correlation of the multi spectral radiances, cloud properties and cloud top pressures. The Cloud top pressure retrieval algorithm dedicated for MERIS uses neural networks. The algorithm can be written as:

$$ctp = \mathbf{s}(W_{out} \# \mathbf{s}(W_{in} \# I)) \quad (1)$$

where ctp is the cloud top pressure, W are the trained weight matrices of the neural net and I is the *input vector* containing the measured radiances as well as the viewing geometry and the surface albedo: $I = [R_0, R_1, \mathbf{J}_{sun}, \mathbf{J}_{view}, \mathbf{j}, \mathbf{a}]$. # denotes a matrix multiplication and \mathbf{s} symbolises a sigmoidal function.

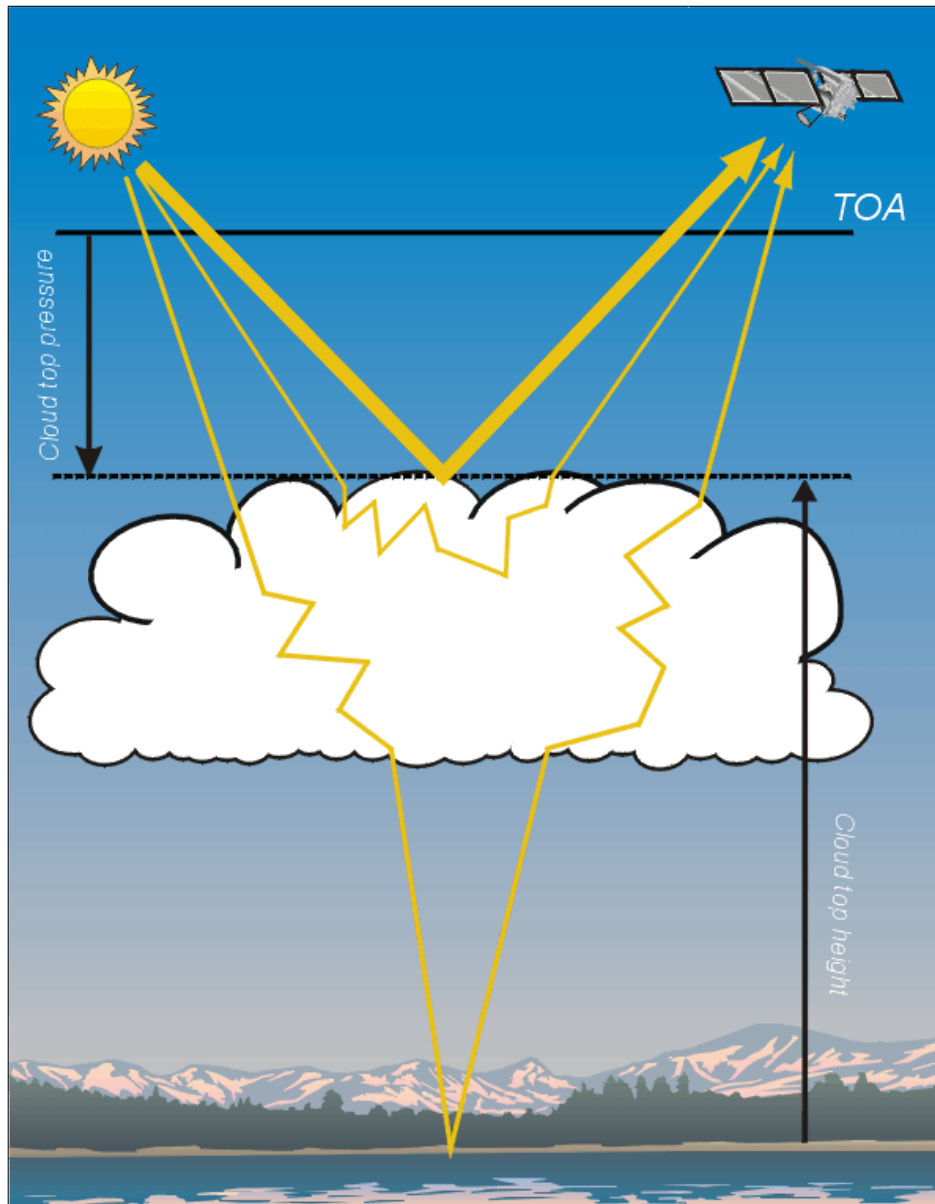


Figure 1: Illustration of the principle of the cloud top height detection using absorption of solar radiation due to well mixed atmospheric gases.

There are several physical parameters which influence the radiance at the O2A-Band:

- the cloud top pressure
- the cloud optical thickness
- the cloud geometrical thickness/ the vertical structure of the clouds
- the possible stratification of clouds
- the temperature / pressure profile
- the surface albedo (spectral and total)
- the effective radius of the cloud particles

Since only radiance measurements at two wavelengths are available but all these parameters are contributing to the measured signals the inversion is strongly underdetermined. This leads to two problems:

1. The inversion can result in non-physical parameter combinations.
2. The accuracy of the inversion is very variable. It is shown in section 3, that the accuracy vary between 10 and 60 hPa depending on the physical parameters.

Problem 2 is fixed by a systematic error analysis based on radiative transfer simulations. An *theoretical accuracy database (tad)* is produced that gives a theoretical retrieval accuracy as a function of the cloud top pressure, the cloud optical thickness and the surface albedo (total). In addition to the cloud top pressure a theoretical accuracy based on this database will be evaluated for each cloudy pixel. Problem 1 will be fixed by a consistency check. Within this check the retrieved cloud optical thickness, the retrieved cloud top pressure and the surface albedo (total) are used for a radiative transfer estimation of the TOA radiances of MERIS channel 10 and 11. The retrieved cloud top pressure is *consistent* if the difference between the estimated and the measured TOA radiances is small. The threshold will be fixed within the validation phase of MERIS. The radiative transfer estimation is made with artificial neural networks.

$$toa_rad = \mathbf{s}(W_{out} \# \mathbf{s}(W_{in} \# I)) \quad (2)$$

W are the trained weight matrices of the neural net and I is the *input vector* containing the retrieved cloud top pressure, the cloud optical thickness as well as the viewing geometry and the surface albedo: $I = [ctp, cot, \mathbf{J}_{sun}, \mathbf{J}_{view}, \mathbf{j}, \mathbf{a}]$. toa_rad is the *output vector* containing the estimated TOA radiances $toa_rad = [R_{10}, R_{11}]$.

3. ALGORITHM DESCRIPTION

3.1 Theoretical Description

3.1.1 Physics of the Problem

The extinction of radiation due to gaseous absorption depends on the absorber mass and on the absorption coefficients within the radiation path. The measured radiance decreases if the photon path within the atmosphere increases. Therefore, the relation between radiances within and outside absorption bands contains information on the absorber mass penetrated by the photons. For a well mixed absorbing gas like oxygen, the total absorption is linear with the total photon path length. The appearance and the position of clouds alter the possible path lengths significantly. Figure 2a and 2b show simulated radiances in the wavelength domain of the O₂A-band for different cloud top pressures. In both figures the enhanced absorption for lower cloud top pressures is clearly shown. For a sun zenith angle $\vartheta_0=0^\circ$ and nadir view, there is only a minor dependency of window radiances on cloud top pressure (**Figure 2** upper). For higher sun zenith angles the effects of aerosol and Rayleigh scattering increase and thus lower intensities in window channels for lower cloud top heights (**Figure 2** lower)

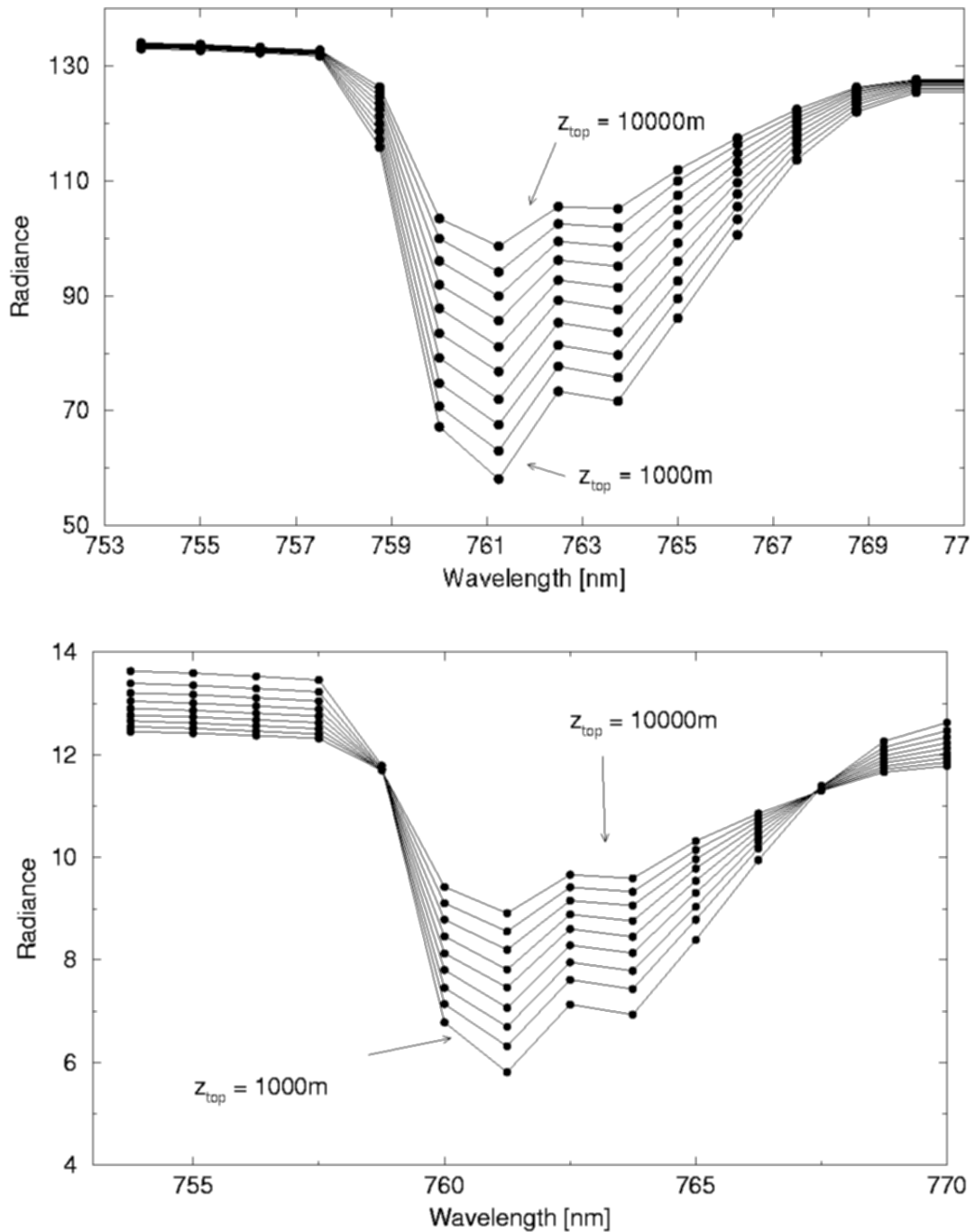


Figure 2: Simulated radiances in the O_2 A-band with different cloud top pressures. Calculations for solar zenith angle $J_0=0^\circ$ (upper) and solar zenith angle $J_0=82.15^\circ$ (lower) and for the cloud parameters: optical thickness $d_c=25$, geometrical thickness $D_z=1000\text{m}$ and effective radius $r_e=8\mu\text{m}$. Radiance values in $\text{W}/\text{m}^2 \text{sr} \mu\text{m}$.

The vertical profile of a cloud affects the radiances within and outside the oxygen absorption band differently. While radiances in window channels only depend on total optical thickness, radiances within the absorption band are also related to the vertical distribution of liquid water.

Photons penetrating into deeper cloud layers have a higher probability of becoming absorbed. In **Figure 3** the ratio of simulated radiances at $\lambda=760\text{nm}$ and $\lambda=753.75\text{nm}$ is shown in a polar plot and a principal plane representation. The left and right side of the Figure belong to the same cloud optical properties and cloud top pressure but they differ in geometrical thickness of the clouds ($\Delta z=1\text{km}$ and 4km). The ratio of radiances at $\lambda=760\text{nm}$ and $\lambda=753.75\text{nm}$ is smaller for clouds with a larger geometrical thickness because the photons penetrate into deeper cloud layer.

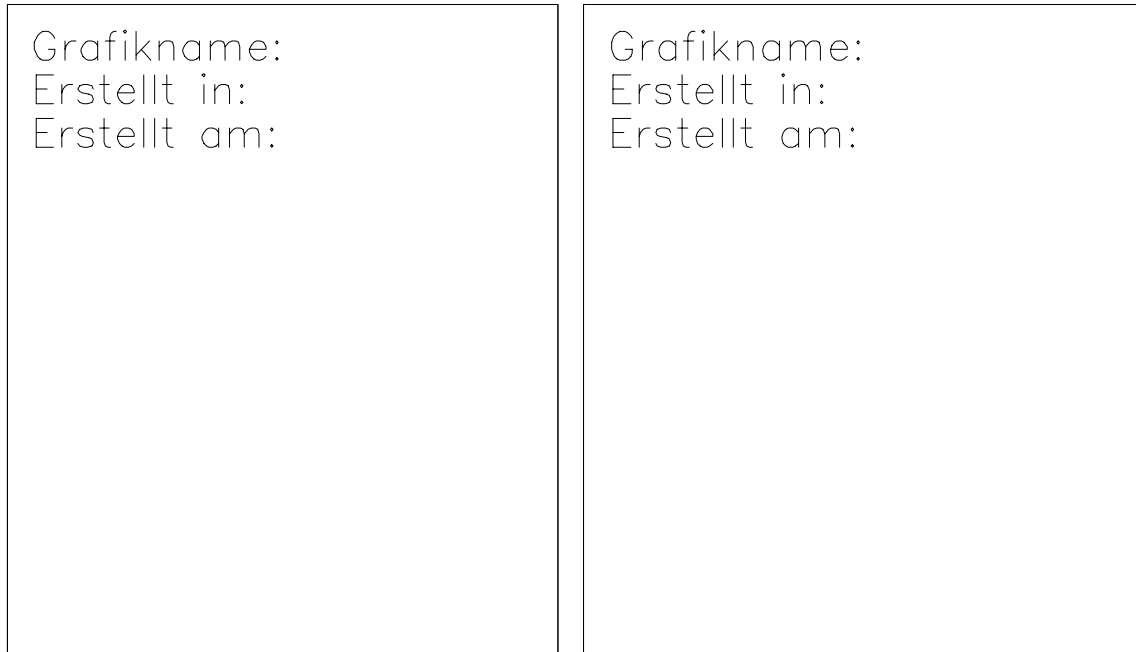



Figure 3: Polar plot and principle plane graph of the simulated field of the ratio between radiances in the O₂ A-band at $\lambda = 761\text{nm}$ (bandwidth $\Delta\lambda = 1.25\text{ nm}$) and in the window channel at $\lambda = 753.75\text{nm}$. Calculations are done for solar zenith angle $J_0 = 35^\circ$ and for cloud parameters: optical thickness $\tau_c = 20$, cloud top height $z_{top} = 10\text{km}$ and effective radius $r_e = 8\mu\text{m}$. The geometrical thickness is $\Delta z = 4\text{km}$ (left) and $\Delta z = 1\text{km}$ (right).

The information on the penetration depth is required for a precise cloud top pressure retrieval. The penetration depth can be taken into account by using additional measurements within the absorption band (Fischer and Graßl, 1991). Depending on the wavelength the absorption in the O₂ A-band differ and the radiation penetrates to different depths within the cloud. During the ESA ELAC '90 aircraft campaign 160.000 multi spectral radiance measurements within the O₂ A-band were taken with a spectral resolution of 0.4nm above different types of clouds over Europe (Fischer and Kollewe, 1994). According to a multivariate analysis three independent quantities for the cloud top pressure retrieval could be identified, which are related to three channels, two within and one outside the absorption band. The photon penetration was found to be the most challenging process to account for and to predict within the retrieval scheme. The vertical distribution and the size of the cloud droplets, expressed by the liquid water content has to be considered within the algorithm. For typical clouds the liquid water content increases with height above the cloud base until a maximum in the upper half is reached (Pruppacher, 1980). Also, the liquid water content of different cloud types such as stratus, stratocumulus and cumulonimbus differ only by a factor of two as long as the temperature does not exceed 280K (Feigelson, 1984). According to this, the variation of liquid water content and its vertical

	MERIS CTP	Doc : Name : Cloud Top Pressure Issue :1 Rev : 0 Date : 27.03.00 Page : 11 of 29
---	----------------------	--

distribution is limited. LWC profiles for different cloud types have to be considered for the development of the cloud top pressure algorithm.

3.1.2 Mathematical Description of the Algorithm

3.1.2.1 Radiative Transfer Calculations

All approaches for the cloud top pressure retrieval, as proposed in this document are based on radiative transfer calculations. The radiative transfer code MOMO (Fischer and Graßl, 1991; Fell and Fischer, 1995) is used to simulate the radiances in the MERIS channels. This code assumes a plan parallel atmosphere, however any vertical inhomogeneity and media of any optical thickness as well as any spectral resolution can be considered. In order to account for the anisotropically backscattered radiation from clouds, the simulations have to be performed for a wide range of observation geometries. In order to account for the required accuracy in cloud top pressure determination, the model atmosphere is divided into 78 layers.

Since the surface reflection affects the radiance even above thick clouds, variations in surface albedo has to be taken into account. Within the simulations the results of high spectral resolution measurements of various types of surfaces are used (Bowker *et al.*, 1985). Different types of vegetation, soil and snow as well as an ocean surface are considered, whereby the albedo and the albedo slope cover natural occurring values. In particular over vegetation the impact of the position of the red edge on the TOA radiances is included. The reflection at the surface is assumed to be isotropic.

An exponential sum fitting technique for transmission (ESFT) is used to incorporate gaseous absorption (Armbruster and Fischer, 1996). The approximation of transmission functions with exponential sums is used for the spectral integration within the radiative transfer code. This is necessary for the integration of the MERIS channels which are influenced by molecular absorption. The calculation of the gas absorption is based on the HITRAN dataset (Rothman *et al.*, 1996), which contains parameters of the single absorption lines of the main atmospheric gases.

The scattering and absorption processes due to aerosols and cloud particles are represented by appropriate scattering and extinction coefficients and the corresponding scattering phase function. These parameters are obtained by Mie theory (Wiscombe 1980). The influence of aerosol scattering is almost negligible in cloudy atmospheres, but the simulations distinguish between the *maritime* and *continental* aerosol types with a constant optical thickness of $\delta_{\text{aero}}=0.125$ at $\lambda=550\text{nm}$ (Toon and Pollack, 1973; WCP 1986). Sensitivity studies have shown, that the influence of varying cloud droplet size distributions $n(r)$ is only of minor importance for the used cloud top pressure retrieval algorithm (Fischer and Graßl, 1991). However various effective radii of cloud droplets were considered. A modified gamma function has been adopted for the cloud droplet size distribution (Hansen, 1971).

The penetration depth in the absorption channels is mainly determined by the relationship between cloud optical thickness, cloud geometrical thickness and cloud top pressure. Therefore varying combinations of the cloud optical thickness, the vertical profile and the cloud geometrical

thickness are considered. The vertical profile of the extinction coefficient is supposed to be ‘triangular’ whereas the maximum appears in the upper half of the cloud. The optical thickness varies between 1 and 350 while the geometrical thickness varies between 0.1 km and 10 km. In that manner, the variability of penetration depth is considered. Therefore the calculations distinguish different cloud types that are specified through the effective radius and ranges of optical thickness, cloud geometrical thickness, extinction coefficients, cloud top pressure and cloud base pressure (Table 1). For this investigation 2000 arbitrary chosen cases are considered.

Table 1: Range of cloud parameters according to the cloud type

Cloud Type Effective Radius (μm)	Cloud Top Height (m)	Cloud Base Height (m)	Cloud Thickness (m)	Extinction (km^{-1})	Cloud Optical Thickness
stratus I 17	100-1500	30-800	100-500	15-20	2-8
stratus II 10	100-1500	30-800	100-500	15-20	2-8
stratocumulus 17	800-2500	500-2500	250-650	16-24	2-14
stratocumulus 10	800-2500	500-2500	250-650	16-24	2-14
nimbostratus 17	5000- 12000	50-2000	3000-9000	20-30	100-250
altostratus 8	4000-7500	3000-6000	500-1500	15-20	8-22
cumulus 25	600-3500	500-2500	300-1000	15-20	8-22
cumulonimbus 33	6000- 12000	800-2000	4000-10000	25-35	150-350
altocumulus 8	3500-6500	3000-6000	400-600	16-24	8-22
stratified stratus + altostratus I	4000-7500	30-800	1000-5000	16-24	20-100
stratified stratus + altostratus II	4000-7500	30-800	1000-5000	15-20	20-100

3.1.2.2 Neural Networks

Artificial neural networks are structures composed of individual processing elements called units or neurones. Neurones are connected with each other by links wearing weights. The used type of network consists of a succession of layers of neurones where every neurone of a certain layer is connected to all neurones of the previous and the next layer. The first layer is used as an input layer, the last layer as an output layer. The layers between input and output layer are called hidden layers. The neurones of the hidden and the output layer transform an incoming signal by applying a sigmoidal function σ :

$$s_t(x) = \frac{1}{1 + e^{-tx}} \quad (3)$$

where t is the ‘temperature’ parameter of the activation function. The connection between the layer n and $n+1$ is represented by the *weight matrix* W_n where each element w_n^{ij} represents the weight of the connection from the i -th neurone in layer n to the j -th neurone in layer $n+1$. Figure 4 illustrates the structure of a neural network with three layers. For a n layer network the processing can be written as:

$$Output = s(W_n \# s(\dots s(W_2 \# s(W_1 \# Input))\dots)) \quad (4)$$

An input vector is transformed into an output vector by a sequence of linear and non-linear transformations. The linear transformation is a matrix multiplication with W_i denoted by #.

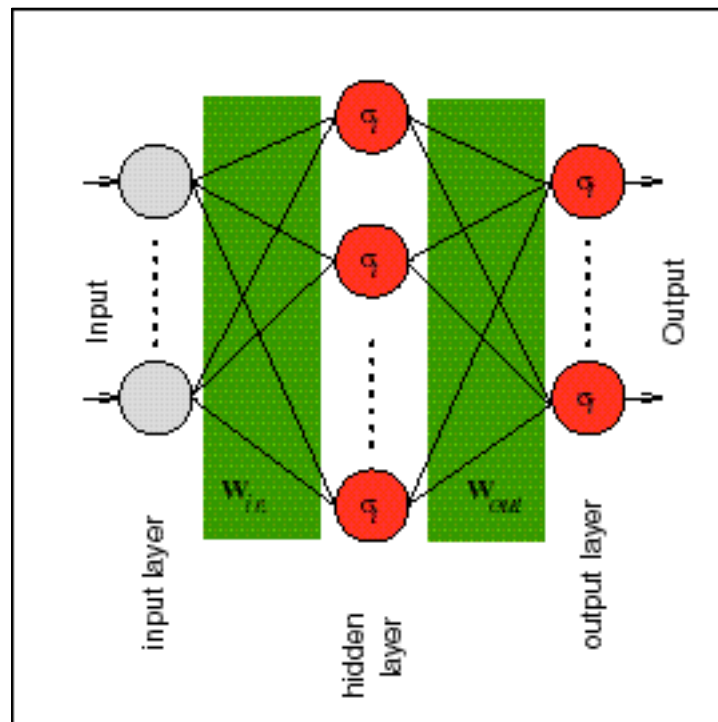



Figure 4: Structure of a neural network with one hidden layer

The neural network learning problem is to find the connection weight matrices W_i . Within the *backpropagation* algorithm it consists of the following steps (Rumelhart, 1986):

1. Initialisation of the matrices with random numbers.
2. Procession of one or more training patterns with the neural net.
3. Calculation of the difference between retrieved output and original output of the training pattern.
4. *Propagation* of the difference *back* through the network and evaluation of the gradients W_{cor_i} .

 Institut für Weltraumwissenschaften	MERIS CTP	Doc : Name : Cloud Top Pressure Issue :1 Rev : 0 Date : 27.03.00 Page : 14 of 29
--	----------------------------	---

5. Correction of the weight matrices by: $W_i = W_i + \gamma W_{cor_i}$. γ is the learning parameter

Steps 2-5 are performed with all training patterns until weights are found which minimise the over all error for a test data set. An independent test data set is necessary to avoid *overtraining* (Rojas, 1993). In the last years this kind of neural net training has been successfully adapted to remote sensing (Lee *et al.*, 1990; Churnside *et al.*, 1994). As for every other inversion algorithm the choice of the training and test data sets is of major importance to ensure reliable results.

For the cloud top pressure retrieval a three layer neural network is implemented. The input contains the TOA reflectance of the MERIS Channels 10 (753.75nm) and 11 (760nm) the sun zenith angle, the viewing zenith angle, the azimuth difference and the albedo of the underlying surface. Two different networks are implemented according to two possibilities: the cloud is over open ocean and therefore the surface albedo is assumed to be zero or the cloud is above land.

3.1.2.3 Inversion

As outlined in Section 4.1 it is indispensable to account for wavelength shifts of channel 11. The spectral mislocation depends on the camera as well as on the field of view within each camera. It can not be avoided but measured in prelaunch. The strategy to overcome the serious consequences is to establish several algorithms for several wavelength shifts. How precise the shift has to be considered is still under examination.

Figure 5 gives an overview on the cloud top pressure algorithm that account for the spectral mislocation. The general form of the retrieval kernel is given in equation (1). The input vector contains the reflectance in the MERIS channel 10, 11 and the viewing geometry: sun zenith, viewing zenith and azimuth. In the case of measurements above land surfaces the albedo is additionally contained in the input vector. The pixel number and the camera identification will be used to estimate the spectral mislocation of the considered pixel from a database prepared before launch. The mislocation and the land sea flag will be used to select an appropriate neural net.

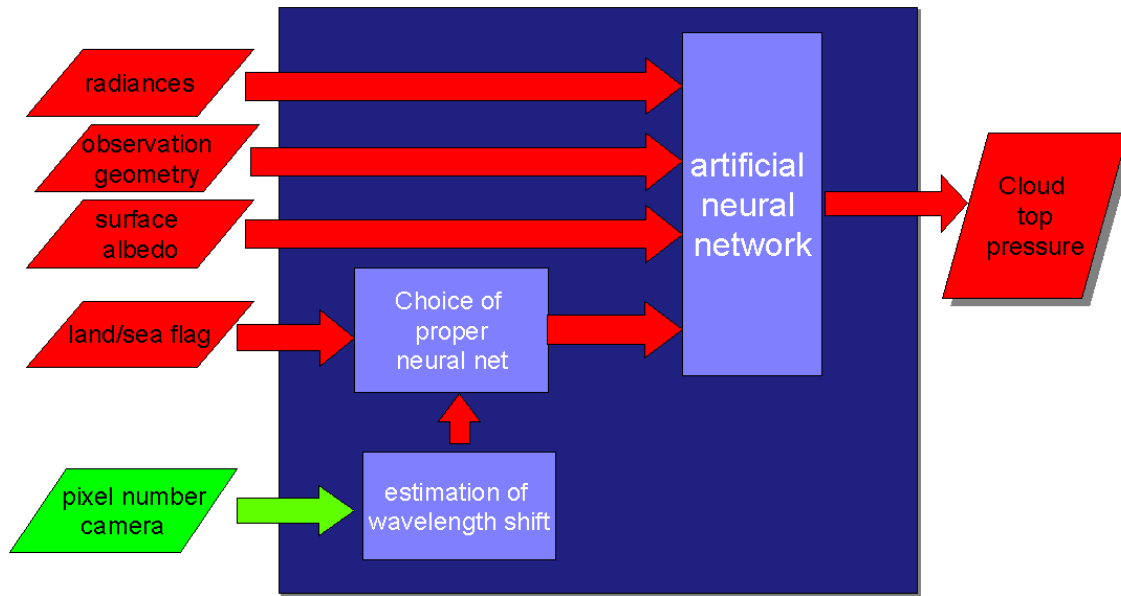


Figure 5: Set-up of the inversion process

3.1.2.4 Generation of the theoretical accuracy database

The *theoretical accuracy database (tad)* consist of a root mean square error (*rmse*) for every combination of cloud top pressure, cloud optical thickness and surface albedo. The *rmse* is evaluated by testing the ctp algorithm with simulated radiances. Therefor the *tad* is theoretical in contrary to the real accuracy which depends additionally on many parameters like the heterogeneity of the surface, 3D effects within clouds, partly cloudy pixels et cetera. The cloud top pressure, the cloud albedo and the surface albedo have been separated into five classes (Table 2). The combinations of low and thick clouds that lead to non-physical extinction coefficients have been dropped (Table 3). For each of the remaining 90 combinations of *ctp*, *cot* and α 20 radiative transfer calculations have been made. The atmospheric parameters have been arbitrarily chosen within the limits given in Table 1 and Table 2.

Table 2: Sample points of the *theoretical accuracy database*

Class	1	2	3	4	5
ctp [hPa]	>950	950-850	850-750	750-500	<500
cot [1]	5-10	10-15	15-25	25-40	>40
α [1]	0.0-0.1	0.1-0.3	0.3-0.5	0.5-0.7	>0.7

Table 3: Matrix of allowed(+) and non-physical(-) combinations of the ctp and cot classes.

	cot 1	cot 2	cot 3	cot 4	cot 5
ctp 1	+	-	-	-	-
ctp 2	+	+	+	-	-
ctp 3	+	+	+	+	-
ctp 4	+	+	+	+	+
ctp 5	+	+	+	+	+

The results of the radiative transfer calculations have been used as a test data set of the cloud top pressure algorithm. The *rmse* of each sample point have been evaluated by:

$$rmse(ctp, cot, \mathbf{a}) = \sqrt{\frac{\sum_{i=1}^n (ctp_{true}(ctp, cot, \mathbf{a}) - ctp_{retrieved}(ctp, cot, \mathbf{a}))^2}{n}} \quad (5)$$

3.1.2.5 Consistency check by estimation of the TOA radiance

Within this check the retrieved cloud optical thickness, the retrieved cloud top pressure and the surface albedo (total) are used for radiative transfer estimation of the TOA radiances in MERIS channel 10 and 11. The retrieved cloud top pressure is *consistent* if the difference between the estimated and the measured TOA radiances is small. The difference *cm* is the consistency measure.

$$cm = \left\| \frac{es_toa_rad - me_toa_rad}{me_toa_rad} \right\| \quad (6)$$

$es_toa_rad = [R_{10}, R_{11}]$ are the estimated radiances and $me_toa_rad = [R_{10}, R_{11}]$ are the measured radiances at TOA. A threshold for *cm* will be defined within the validation phase of MERIS. A radiative transfer calculation is much too time consuming for operational purpose. Instead of this an estimation is made with artificial neural networks.

$$es_toa_rad = \mathbf{s}(W_{out} \# \mathbf{s}(W_{in} \# I)) \quad (7)$$

W are the trained weight matrices of the neural net and I is the *input vector* containing the retrieved cloud top pressure, the cloud optical thickness as well as the viewing geometry and the surface albedo: $I = [ctp, cot, \mathbf{J}_{sun}, \mathbf{J}_{view}, \mathbf{j}, \mathbf{a}]$. The database for the training of the estimation algorithm is the same as for the cloud top pressure algorithm.

3.2 Practical Considerations

3.2.1 Numerical computation considerations

The size of the matrices for the neural network approach depends on the number of hidden neurones. Likely numbers are between 15 and 50 neurones. That corresponds to sizes between 2kB and 5kB for each neural net.

The procedure does not contain iterative loops.

3.2.2 Calibration and Validation

A validation of the MOMO model has been carried out with measurements (Fischer *et al.*, 1991) as well as with other radiative transfer simulations for which good agreements are found (Heinemann and Gentili, 1995; Fell and Fischer, 1995). A comparison of MOMO results with high spectral resolution measurements of OVID is shown in Figure 6. The spectra were recorded during EUCREX '95 above a stratus cloud above the Atlantic in the vicinity of Brest, France. The measured spectrum (average spectrum and standard deviation in the grey area) could well be described with the MOMO model (thick line) when using *in situ* measured cloud particle size distribution ($r_c=9\mu\text{m}$) and estimated optical thickness ($\delta_c=20$). For the radiances in the window regions and in the absorption band of water vapour and oxygen we found a very good agreement. Further experimental investigations, particularly in the MERIS commissioning and operational phase, are strongly recommended and will provide opportunities for validation and algorithm

refinements. Radiance measurements should be accompanied by *in situ* observations and with LIDAR measurements for accurate cloud top pressure determination.

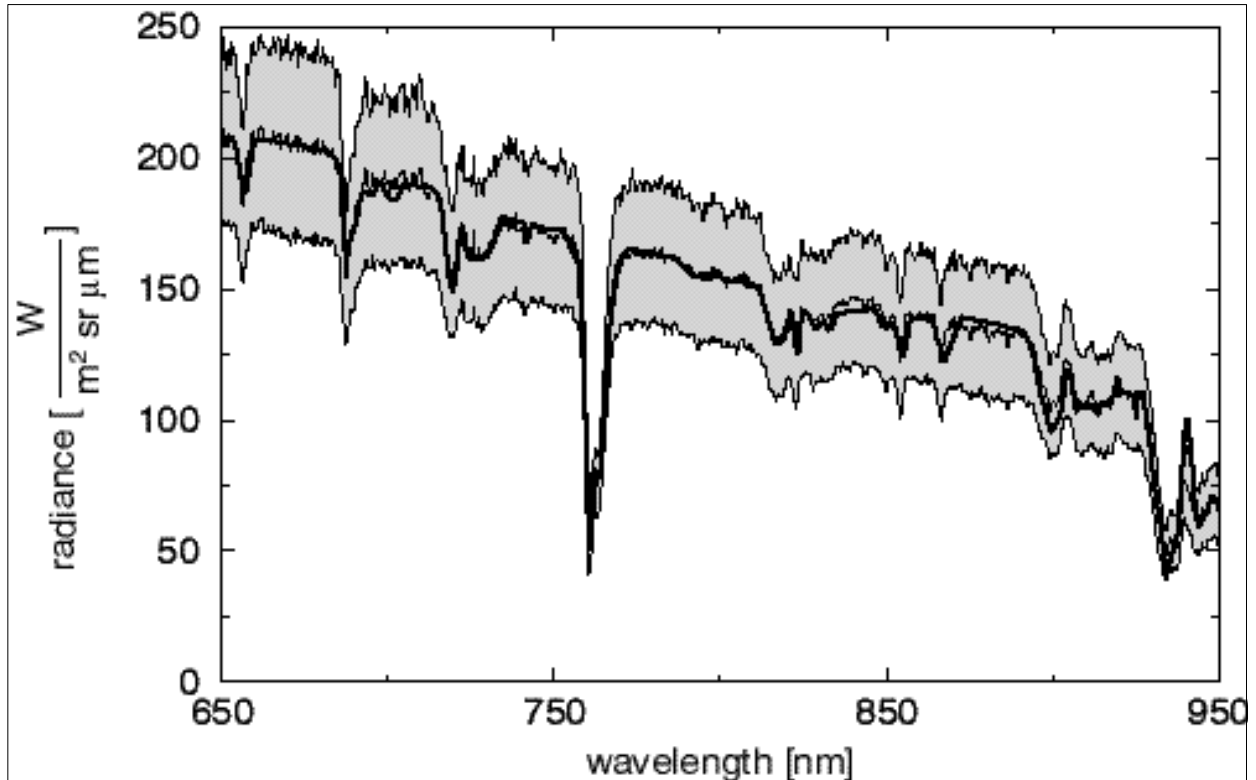


Figure 6: Comparison between measured and simulated radiances above clouds. The averaged measured radiance and its standard deviation is denoted with the shadowed area. The spectra were recorded with the high resolution multi channel spectrometer OVID during EUCREX '94 above a stratocumulus field. The thick line is the simulated spectrum calculated with the cloud parameter $d_c=20$, geometrical thickness $D_z=600m$, cloud top height $z_{top}=1100m$ and effective radius $r_e=9\mu m$.

Simultaneous measurements of the cloud top heights and the radiance in the O2A band as performed during the CLOUDYCOLUMN mission (Brenquier 1990) of the Aerosol Characterisation Experiment (ACE2) 1997 enable the validation of the algorithm. During this mission two aircraft, one equipped with a LIDAR and the other with OVID flew a correlated flight pattern above a stratocumulus deck. An cloud top pressure algorithm adapted to OVID channels and to a flight height of 10000Ft was used to estimate the cloud top height. An excellent agreement has been found (**Figure 7**).

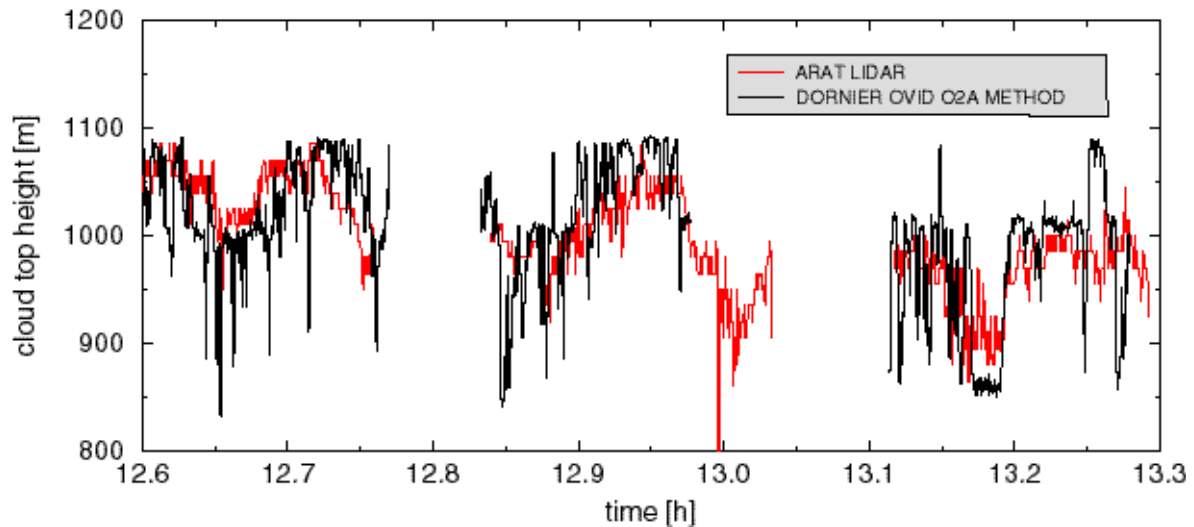


Figure 7: Measurements of the cloud top heights from two aircraft., one equipped with a LIDAR (red lines) the other with a OVID. The radiance measurements have been used to estimate the cloud top height (black lines).

3.2.2.1 Quality Control, Diagnostics and Exception Handling

The sensitivity tests for the algorithms indicate measurement situations and measurement errors for which the algorithm is less reliable. The algorithm will be applied only for pixels that are indicated as cloudy by the cloud screening algorithm. Pixels for which the quality control failed, will pass the algorithm without result.

If the algorithm receives or retrieves parameters, that lies outside realistic boundaries (defined by the radiative transfer calculations), a quality flag will be raised, indicating, what bond was exceeded. For that specific pixel, no cloud parameter will be estimated.

3.2.2.2 Output Products

cloud top pressure[hPa], theoretical cloud top pressure accuracy [hPa], consistency measure[1]

4. ERROR BUDGET ESTIMATES AND SENSITIVITY TESTS

The ill posed nature of the inversion as well as the shortcomings of radiative transfer modelling and instrumental characteristics will affect the accuracy of the cloud top pressure algorithm. Sensitivity studies on the influence of these errors have been performed to acquire the most sensitive properties of the algorithm. The *rmse* and the *bias* are used to characterise the accuracy.

$$rmse = \sqrt{\frac{\sum_{i=1}^n (ctp_{true} - ctp_{retrieved})^2}{n}} \quad (8)$$

$$bias = \frac{\sum_{i=1}^n (ctp_{true} - ctp_{retrieved})}{n} \quad (9)$$

4.1 Sensitivity to band setting and to spectral registration

The spectral mislocation of the channels can significantly influence the accuracy of the retrieved cloud top pressure. The O₂ A-band absorption causes a strong sensitivity especially of Channel 11. The spectral mislocation depends varies from camera to camera and depends on the relative viewing angle (**Figure 8**).The mislocation can not be avoided thus its influence has to be considered in the algorithm. This can be realised by an optimal band setting of Channel 11 and by an inclusion of the spectral registration into the cloud top pressure algorithm.

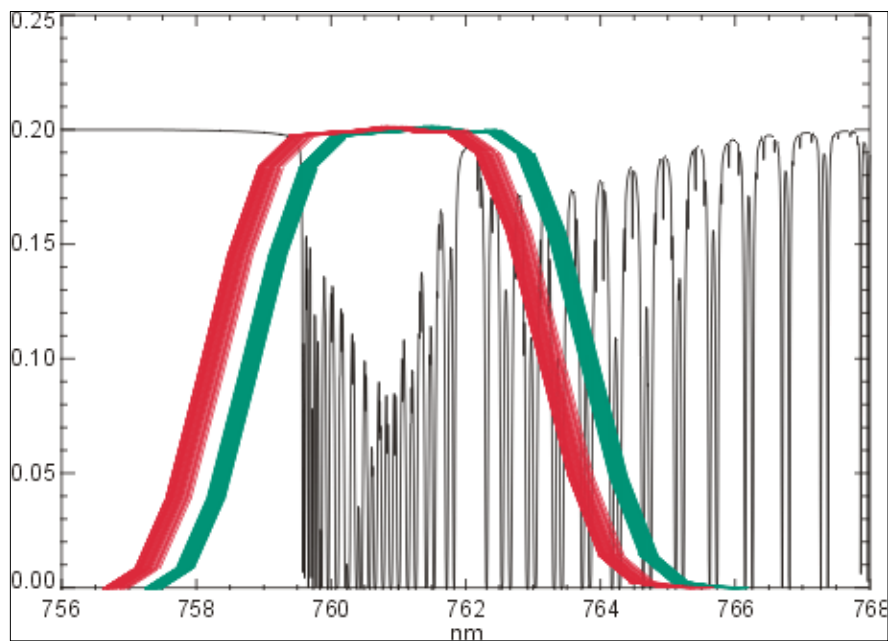


Figure 8: Spectral response functions of several MERIS pixels of channel 11 together with the transmission of oxygen. The green curves belong to camera 3 and the red curves belong to camera 5. The variation within one camera is due to the variability of the channel response within the field of view of a camera ('smile effect').

4.1.1 Optimal band setting deduced from experimental data

To find an optimal band setting two possibilities within the restriction of the MERIS sensor have been examined. 10000 radiance spectra ($\Delta\lambda=0.3\text{nm}$), taken with the high resolution airborne spectrometer OVID above stratocumulus clouds, have been used to simulate MERIS measurements. Channel 11 has been considered to consist of two spectral MERIS pixels ($\lambda_c \approx 760.0 \text{ nm}$ $\Delta\lambda \approx 2.5 \text{ nm}$) as well as of three spectral MERIS pixels ($\lambda_c \approx 760.8 \text{ nm}$ $\Delta\lambda \approx 3.75 \text{ nm}$) (Figure 9).

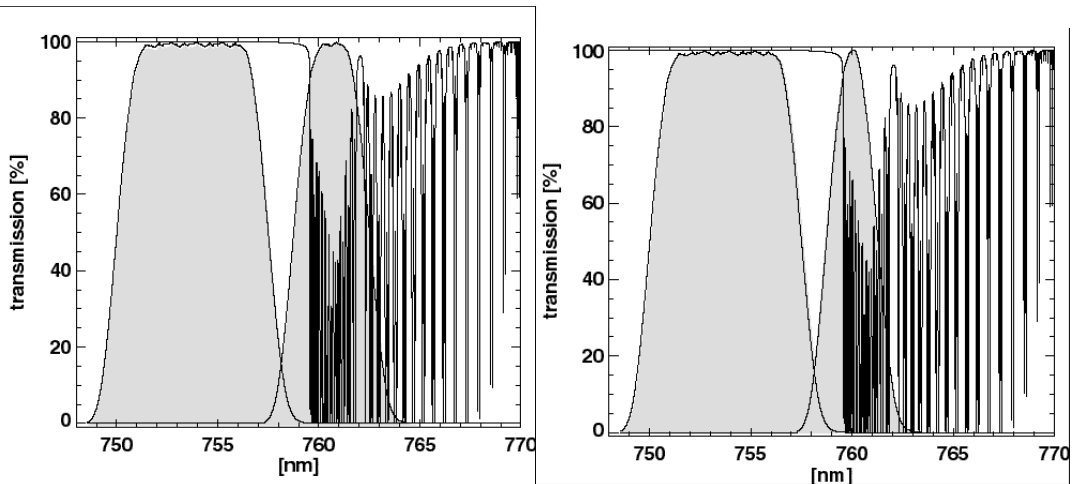


Figure 9: Definition of the MERIS Channels 10 and 11 and the transmission of oxygen for a 'midlatitude summer atmosphere'. In the right picture channel 11 consists of two spectral elements and in the left picture of three spectral elements of MERIS.

Additionally all channels have been simulated with a shift of the centre wavelengths of ± 1 nm in steps of 0.2 nm. The radiance deviation which results from this wavelength shifts are shown in Figure 10. Channel 11 is less sensitive if it consists of 3 pixels. This will be affirmed within the next section.

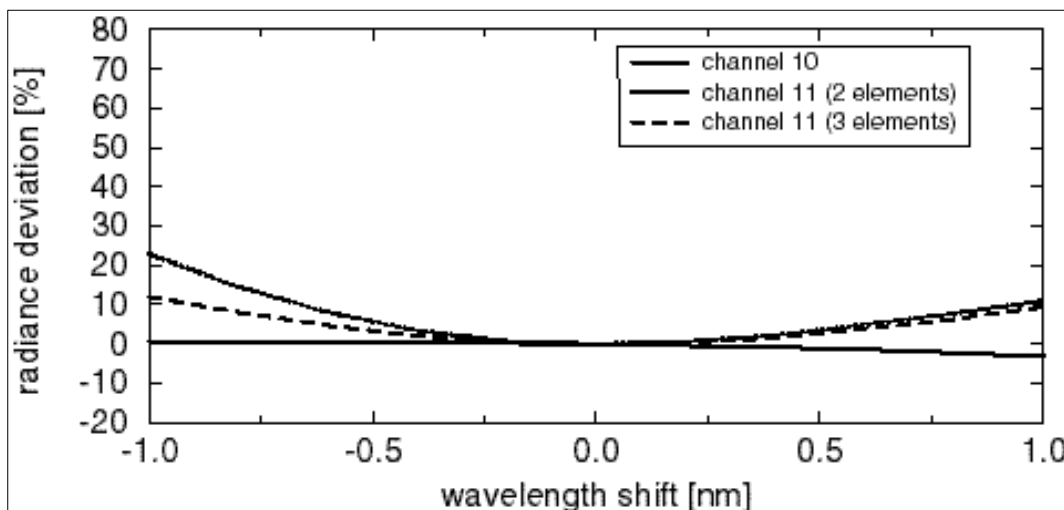


Figure 10: Radiance deviation within the MERIS channels 10 and 11 as a function of a wavelength shift.

4.1.2 Optimal band setting deduced from simulated data

The choice of the optimal band setting must depend on the algorithm performance as well. The overall performances were tested with respect to the noise sensitivity. There are uncertainties in the radiance due to the signal to noise ratio of the instrument. According to the gain settings in the cloud channels a noise equivalent radiance (NEAR) of $0.2 \text{ W}/(\text{m}^2 \text{sr } \mu\text{m})$ at a maximum radiance of about $400 \text{ W}/(\text{m}^2 \text{sr } \mu\text{m})$ is specified for MERIS (ESA, 1995). A TOA radiance of $30 \text{ W}/(\text{m}^2 \text{sr } \mu\text{m})$ in channel 11 expresses a reasonable lower limit. This would lead to signal noise

of about 1%. To consider a bandwidth of realistic conditions the signal noise was varied between 0% and 1.5% in steps of 0.25%. At each signal noise level the modified test data were processed with the trained neural net. (**Figure 11** black lines). No significant differences have been found between the two band settings. Additionally the test was made for data considering the variability of the spectral channel definition within the field of view of a camera (**Figure 11** blue lines). Again, as outlined in the previous section, the band setting of Channel 11 consisting of 3 MERIS pixels is less sensitive and therefore preferred.

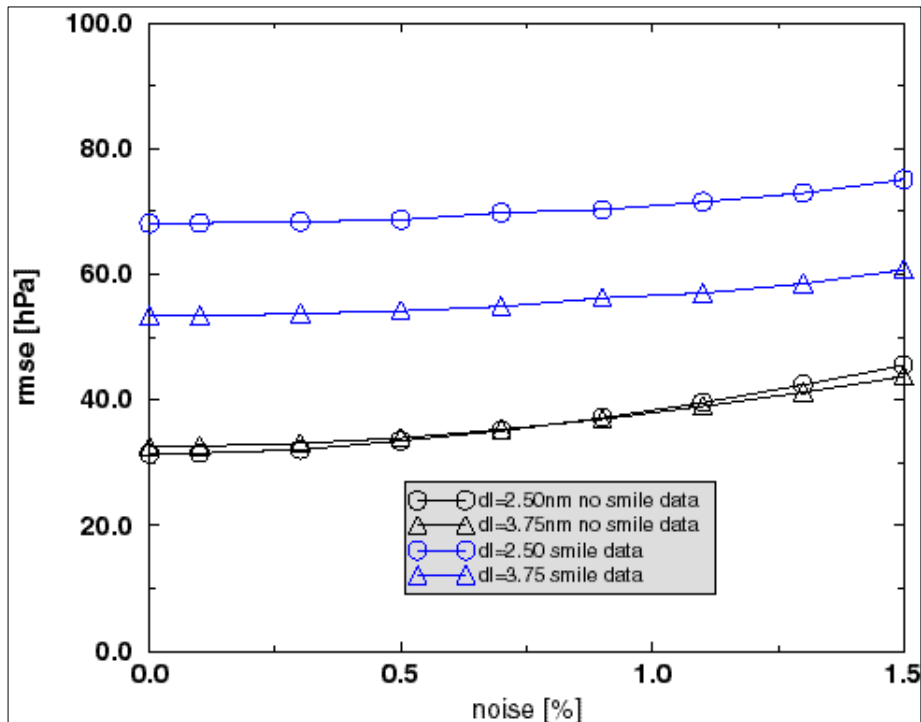


Figure 11: Root mean square error (rmse) of the retrieved cloud top pressure with (black) and without (blue) considering the variability of the spectral channel definition within the field of view of a specified camera ('smile effect')

Even though the influence of the smile to the algorithm accuracy can be reduced it is still unacceptable large. The overall rmse increases from about 35 hPa to 55 hPa.

But the variation due to the smile are smaller than the variations due to different cameras (**Figure 8**). The latter can effect an overall *inaccuracy* of up to 200 hPa (Figure 12). Here the algorithm produced senseless values.(For the special case of camera 3 the 2.5 nm variant is 'less' sensitive than the 3.75 nm variant but still senseless). It is therefore indispensable to include the spectral mislocation into the algorithm.

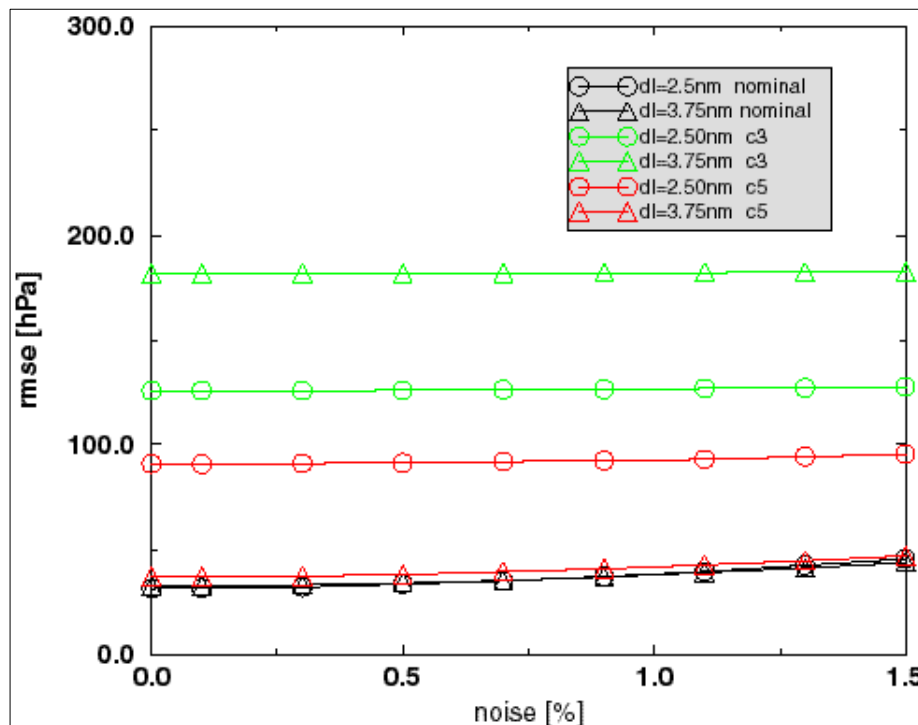


Figure 12: Root mean square error (RMSE) of the retrieved cloud top pressure as a function of instrumental noise for the nominal channel definition of MERIS of channel 11 (black), for camera 3 and camera 5. Circles are indicating bandwidths of 2.5nm and triangles are indicating bandwidths of 3.75nm.

4.2 Classification of the cloud top pressure algorithm error

All investigations described in the following sections have been made for an instrumental gaussian noise of 0.5% to account for realistic conditions. Additionally they have been repeated for a band-setting of +/-0.1nm. The results show absolutely no differences to the nominal channel definition. Therefore an algorithm that account for the spectral mislocation is able to neutralise this effect. The required accuracy of the spectral registration knowledge is under investigation.

4.2.1 Absolute Calibration

The requirements for the absolute calibration are under examination

4.2.2 Sensitivity to surface albedo and cloud optical thickness

The influence of the surface to the reflectance at top of atmosphere and therewith the accuracy of the cloud top pressure algorithm increased with decreasing cloud optical thickness and increasing surface reflection. Especially a combination of thin clouds over bright surfaces leads to an overestimation of the cloud top pressure and thereby to an increasing algorithm error. For moderate optical thickness and surface albedo the bias is neglectable. The rmse is below 30hPa for most the cloud and surface reluctance usually occur. This is due to the ambiguity of the inverse problem according to cloud optical thickness, surface albedo and penetration depth. (Figure 13)

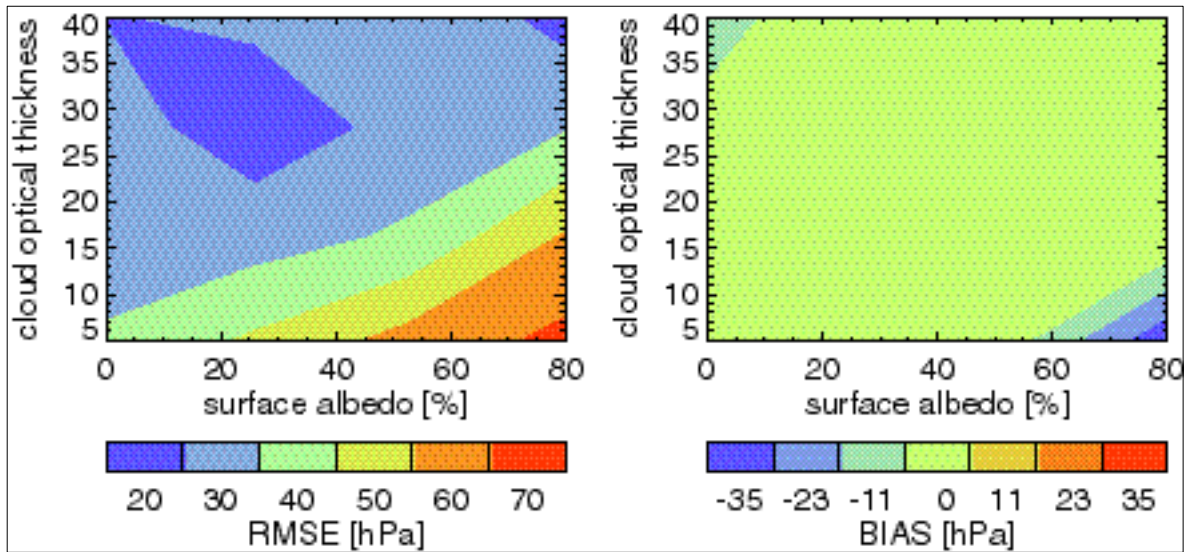


Figure 13: Sensitivity of the ctp algorithm to cloud optical thickness and surface albedo. A negative bias (blue) means overestimation of the cloud top pressure.

Since the surface albedo can only be known to a certain accuracy the surface albedo of the test data was varied to study this influence. Errors in the albedo of up to 0.2 (rmse) have been simulated.(**Figure 14**) Again thin clouds and bright surfaces are the most sensitive conditions. Considering that the natural occurrence of thin clouds is higher than of thick clouds the precise knowledge of the surface albedo is a key factor for the ctp accuracy.

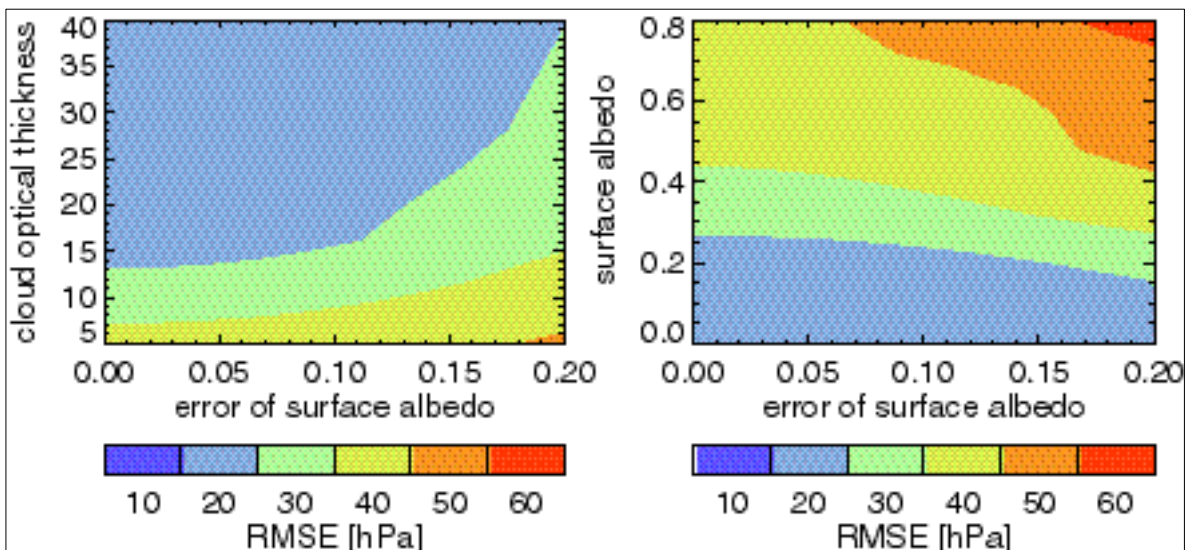


Figure 14: Sensitivity of the ctp algorithm to the error of the surface albedo as a function of the cloud optical thickness (left) and the surface albedo (right).

4.2.3 Sensitivity to cloud optical thickness and cloud top pressure

As outlined in the last section the accuracy of the ctp algorithm decrease with decreasing cloud optical thickness since the influence of the surface increases. The impact is different for different cloud top pressures. The cloud top pressure of low thin clouds will be underestimated in contrary

to higher (between 800 hPa and 700 hPa) thin clouds which will be overestimated (**Figure 15** right). As in the previous section the reason is the ambiguity of the inverse problem according to cloud optical thickness, surface albedo and penetration depth. This leads to an rmse of the retrieved ctp of up to 55 hPa (red areas in **Figure 15** left), which is substantially higher than the overall rmse of 33hPa.

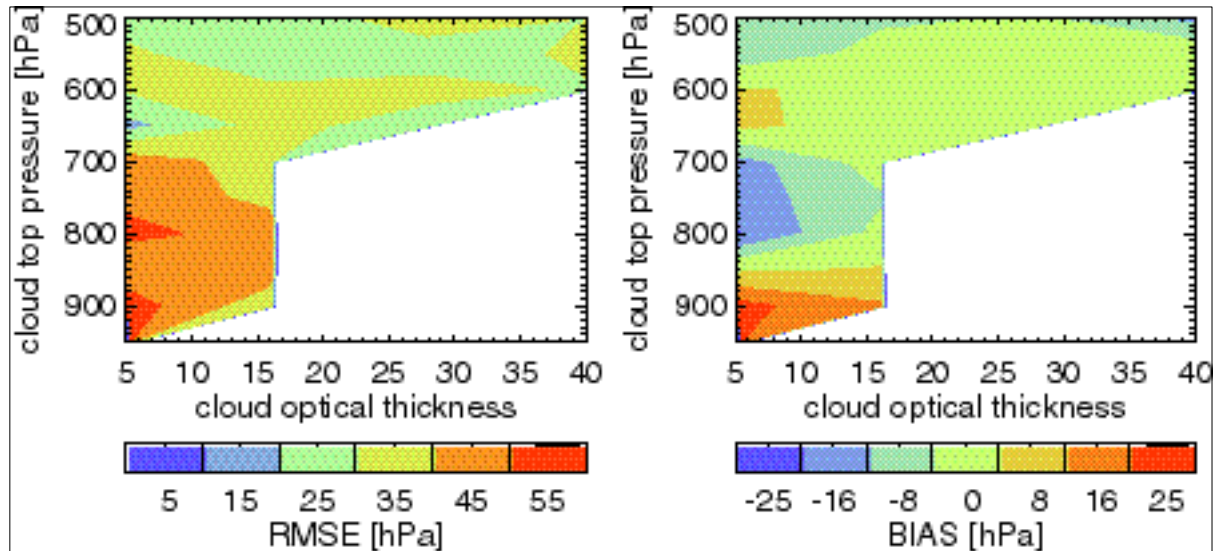


Figure 15: Sensitivity of the cloud top pressure retrieval to cloud optical thickness and cloud top pressure. The white areas are not represented in the test and training database.

4.2.4 Sensitivity of the cloud top pressure retrieval to viewing and solar zenith angle

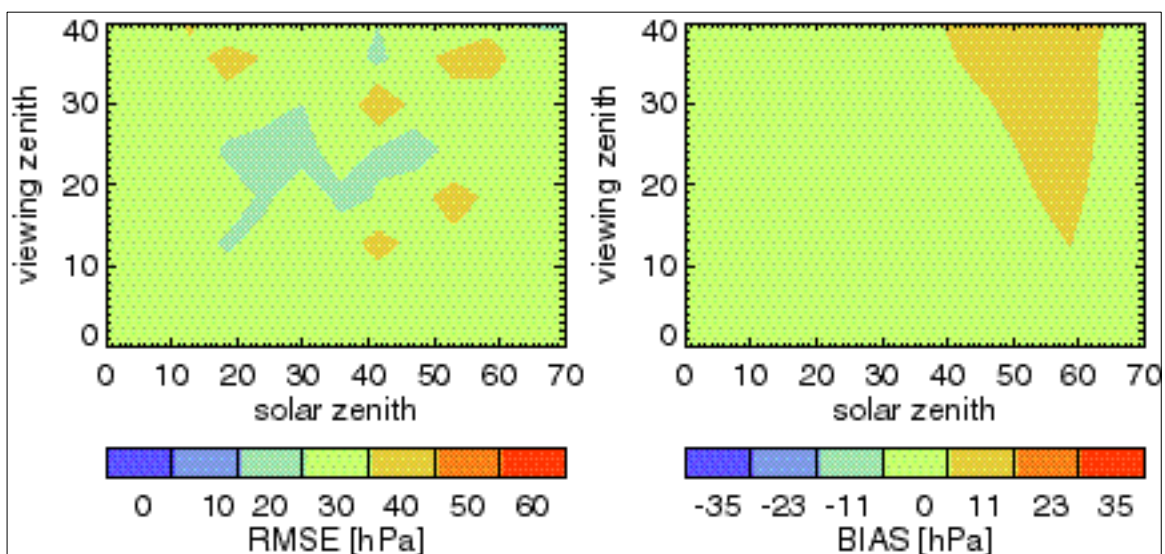


Figure 16: Sensitivity of the cloud top pressure retrieval to viewing and solar zenith angle.

Figure 16 shows the rmse and the bias of the retrieved cloud top pressure as a function of the viewing zenith and the solar zenith angle. The rmse has no significant dependence on the viewing geometry whereas the bias shows increases towards high solar zenith and viewing zenith angles.

4.2.5 MERIS swath simulation

The clear representation of all the cloud top pressure accuracy influencing parameters together is quite difficult. A simple solution is to limit the range of parameters to values as they occur during a representative MERIS swath.

Two steps are performed to access the quality of the algorithm. Firstly, the radiance values for each pixel of the swath have been computed by using radiative transfer simulations of MERIS Channel 10 and 11. In a second step, the cloud top pressure algorithm has been applied to these pseudo MERIS images. Projections of the swath images to a map should help to identify geographic regions, where the retrieval is critical.

The properties of the considered MERIS swath simulation are listed in Table 3. This particular swath has been selected, because it covers areas over ocean (70% of all pixels) and land surfaces of different reflectivity (30 % of all pixels) which is quite representative for the land-ocean coverage fraction of the whole earth. The orbital parameter of ENVISAT and the viewing geometry of the MERIS sensor has been used to calculate longitude and latitude as well as the solar and viewing zenith angle and the azimuth difference of each pixel.

Table 4: Properties of the considered MERIS swath.

Day of the year	80
Measuring time	1100 sec
Satellite inclination	1,72°
Satellite altitude	799 km
Equator crossing time	10:00
Latitude range	70°N – 55°S
Longitude range	15°E – 29°W
Solar zenith angle range	26° - 71°
Viewing zenith angle range	0° - 40°
Azimuth difference range	0° - 180°
Surface albedo range	0% - 40%

The land surface albedo is taken from the data-set of the *International Satellite Land Surface Climatology Project ISLSCP* (Sellers *et al.* 1995). The surface albedo is an integrated value over the entire solar spectrum, thus no wavelength dependencies are considered. Because of the very large solar zenith angles in the northern and southern part of the swath where an estimate of cloud top pressure, cloud optical thickness and cloud albedo is not possible, we restricted our analysis to the range between 70° N and 55° S latitude.

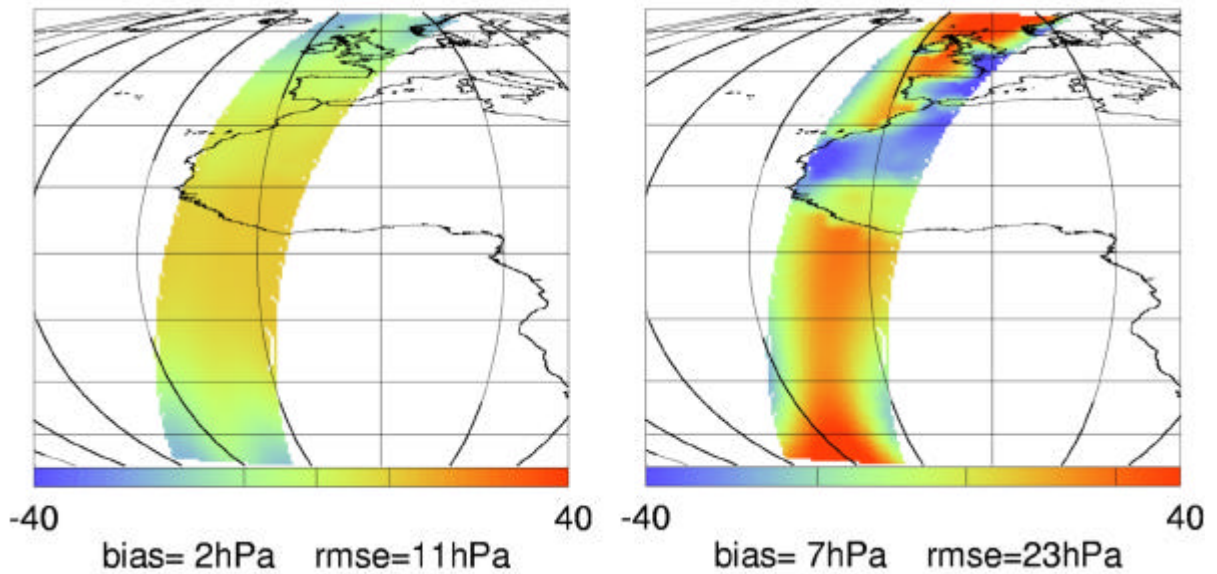


Figure 17: Absolute difference of the retrieved cloud top pressure to the cloud top pressure used to calculate the MERIS swath. Radiances have been calculated with a cloud top pressure of 550hPa and an optical thickness of $d_c = 20$ (left) and with a cloud top pressure of 855 hPa and a cloud optical thickness of $d_c = 8$ (right).

The error of the cloud top pressure retrieval across the MERIS swath is shown in **Figure 17**. For an optical thickness of $\delta_c = 20$ the overall rmse is small and the absolute difference between the retrieved cloud top pressure and the cloud top pressure used to calculate the MERIS swath varies slightly. For high solar zenith angles the differences increase (left graph). In contrast, the accuracy for a low cloud optical thickness depends on the viewing geometry and on the surface albedo. A combination of a high surface albedo and a low optical thickness leads to an overestimation (blue areas) of the cloud top pressure whereas the cloud top pressure is underestimated (red areas) above dark surfaces and for high solar zenith angles (right graph).

4.2.6 Accuracy of the TOA radiance estimation

The meaningfulness of the consistency measure cm depends strongly on the accuracy of the neural network radiance estimation. To test this accuracy the cm of the simulated and the estimated radiances of the test data set was evaluated. Figure 18 shows the histogram and the cumulative histogram of evaluated consistency measure. For 99% of the data the accuracy of the estimation is better than 10%. The probability of an inconsistency larger than 10% due to the inaccuracy of the radiative transfer estimation is smaller than 1%. Other reasons like measurement errors, atmospheric situations that can not be simulated with a 1D radiative transfer code or retrieval errors due to the under determination of the inverse problem are much more likely.

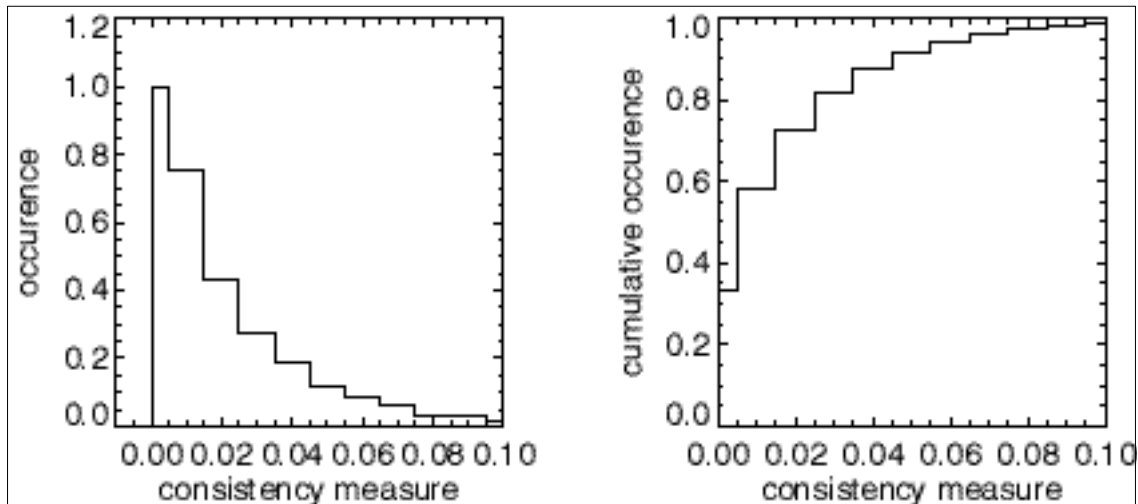


Figure 18: Histogram and cumulative histogram of the frequency of the consistency measure. 30 % of the data has a inconsistency smaller then 1 %. For 99% of the data the accuracy of the estimation is better then 10 %.

5. ASSUMPTIONS AND LIMITATIONS

The algorithm is based on radiative transfer calculations for which a plan parallel atmosphere is assumed. For low sun elevations and high observation angles, the assumption of a plan parallel atmosphere is less fulfilled. Except Monte-Carlo method, there are no 3-dim radiative transfer codes available which could describe the shape of the clouds more realistically. Nevertheless such radiative transfer codes have also significant limitations to describe 3-dim clouds adequately. Effects from non-horizontal homogenous clouds cannot be treated with the MOMO model, but the influence of vertical distribution of cloud appearance are described. The environment effects of neighbourhood pixels cannot be treated with the MOMO model.

6. REFERENCES

Armbruster, W. and J. Fischer, 1996: An improved Exponential Sum Fitting Technique to submitted to *Appl. Opt.*

Bakan *et al.* , 1998: CIVEX Field Phase Report

Brenguier, J.-L., H. Pawlowska, L. Schüller, R. Preusker, J. Fischer, Y. Foucart, 1999: Radiative properties of boundary layer clouds: optical thickness and effective radius versus geometrical thickness and droplet concentration, submitted to *J. Atmos. Sci.*

Churnside, J. H., T. A. Stermitz, J. A. Schroeder, 1994: Temperature Profiling with neural network inversion of microwave radiometer data. *J. Atm. Oc. Tec.*, **11**, 105 -109.

Feigelson, E. M., 1984 Radiation in a cloudy atmosphere, D. Riedel Publishing Company, Dordrecht

Fell, F and J. Fischer, 1995 Validation of the FU Berlin Radiative Transfer Model, to be published in the final report of the EC-Contract MAS2-CT92-0020

Fischer, J., and H. Graßl 1991: Detection of Cloud-Top Height from Backscattered Radiances within the Oxygen A-Band - Part 1: Theoretical Study.- *J. Appl Met.*, **30**, 1245-1259

Fischer, J., W. Cordes, A. Schmitz-Peiffer, W. Renger and P. Mörl, 1991: Detection of Cloud-Top Height from Backscattered Radiances within the Oxygen A-Band Part 2: Measurements. *J. Appl Met.*, **30**, 1260-1267.

Fischer, J. and M. Kollwe, 1994: Study of cloud top height determination using a coarse spatial resolution imaging spectrometer.- Final Report, ESA-ESTEC study, RFQ/3- 7241/91/NL/ BI.

Heinemann, Th. and B. Gentili, 1995 Comparison between Radiances calculated by the Villefranche Monte-Carlo Model and the Berlin Matrix-Operator-Model (MOMO), WP 5000 Radiative Transfer Simulations Preliminary Report

King, M. D., 1987 Determination of scaled optical thickness of clouds from reflected solar radiation measurements. *J. Atmos Sci.*, **44**, 129-144

Lee, J., R.C. Wegner, S.K. Sengputa, and R.M. Welch, 1990: A neural network approach to cloud classification.- *IEEE Transactions on Geoscience and Remote Sensing*, **28** (5), 846-855

Nakajima, T., M. D. King, 1988 Cloud optical parameters as derived from multispectral cloud radiometer. Vale, FIRE Science Experiment Team

Neckel, H. and D. Labs, 1984 Improved Data for Solar Spectral Irradiance from 330 to 1250nm, *Solar Phys.*, **90**, 205-258

O'Brien, D. and R.M. Mitchell, 1992: Error estimates for Retrieval of Cloud-Top Pressure Using Absorption in the A Band of Oxygen. *J. Appl. Meteor.*, **31**, 1179-1192.

Ohring, G. and S. Adler, 1978 Some experiments with a zonally averaged climate model, *J. Atmos. Sci.*, **35**, 186-205

Pruppacher, H. R. 1980 Microstructure of atmospheric clouds and precipitation. *Clouds: Their Formation, Optical Properties and Effects*, P. Hobbs and A. Deepack, Eds. 93-185

Ramanathan, V., R. D. Cess, E. F. Harrison, P. Minnis, B. R. Barkstrom, E. Ahmad, D. Hartmann, 1989 Cloud radiative forcing and climate: Results from the Earth Radiation Budget Experiment. *Science*, **243**, 57-63

Rojas, R. : Theorie der neuronalen Netze: eine systematische Einführung. Berlin, Springer 1993

Rothman, L. S., R. R. Gamache, A. Barbe, A. Goldman, J. R. Gillis, L. R. Brown, R. A. Toth, J.-M. Flaud and C. Camy-Peyret, 1983: AFGL atmospheric absorption line parameters compilation: 1982 edition, *Appl. Opt.*, **22**, 2247-2256

Rumelhart, D. and J. McClelland, 1986 Parallel Distributed Processing. MIT Press, Cambridge, Massachusetts

Toon, O. B. and J. B. Pollack, 1973 A global Average Model of Atmospheric Aerosols for Radiative Transfer Calculations, *J. Appl. Met.*, **15**, 225-246

Yamamoto G., D. Q. Wark, 1961 Discussion of the Letter by R. A. Hanel, Determination of Cloud Altitude from a Satellite. *J. Geophys. Res.*, **66**, 3596

WCP-report No. 112, 1986 A preliminary cloudless Standard Atmosphere for Radiation Computation, WMO/TD-No. 24

Wiscombe, W. J., 1980 Improved Mie scattering algorithm, *Appl. Opt.*, **19**, 15505-1515

Wu, M.-L. C., 1985 Remote Sensing of Cloud-Top Pressure Using Reflected Solar Radiation in the Oxygen A-Band, *J. Appl. Met.*, **24**, 549-546